

Ising Machine based on Bistable Microelectromechanical Systems

Motohiko Ezawa¹, Eric Lebrasseur² and Yoshio Mita²

¹*Department of Applied Physics, University of Tokyo, Hongo 7-3-1, 113-8656, Japan and*

²*Department of Electrical Engineering, University of Tokyo, Hongo 7-3-1, 113-8656, Japan*

We propose an Ising machine made of microelectromechanical systems (MEMS), where the annealing process is automatically executed by a dissipation mechanism. The core structure is a series of buckled plates. Two stable positions of each plate (left and right) represent its binary state acting as a bit so that a plate works as a mechanical memory. The electrostatic interaction between adjacent plates is introduced by applying voltage. Plates continue to flip between two stable buckled positions until the series of plates reaches a local minimum due to the damping of the mechanical motion. First, we design Ising machines simulating a ferromagnetic (FM) interaction and an antiferromagnetic (AF) interaction separately. Then, we propose a fully-connected MEMS network representing a coexistence system of FM and AF interactions in an arbitrary way, by way of which an arbitrary combinatorial problem described by the Ising model can be solved. The present mechanism works at room temperature without external magnetic field, which is very different from the standard classical or quantum annealing mechanism.

I. INTRODUCTION

Many binary-combinatorial problems are described by the Ising model[1]. It is solved by an Ising machine, where a local minimum state is efficiently obtained by an annealing method. There are various ways for the annealing process. A classical way is a simulated annealing[2, 3], where we decrease temperature to obtain a local minimum state. The quantum annealing machine[4–6] is one of the most successful quantum machines on a commercial basis although it is not a universal quantum computer. It determines a local minimum state of a transverse-field Ising model by gradually decreasing the magnetic field. However, it is necessary to cool down the sample below the helium temperature in order to make the system superconducting.

Recently, many variations of the Ising machine are proposed[7] such as a coherent Ising machine[8–12] based on photonic systems, an electronic oscillator-based Ising machine[13], accelerated simulated annealers[14, 15], a simulated bifurcation machine[16, 17] based on digital computer and a probabilistic-bit (p-bit) machine[18–22] based on magnetic systems. The key point is how to make a binary stable state representing the Ising degree of freedom and how to control it. It is advantageous if we are able to construct an Ising machine with the use of current electromechanical technologies.

There is an important observation made by Feynman[23]. He proposed to use the equations of motion describing a natural phenomenon to solve a given problem in the context of quantum computations. The execution is done all at once at high speed. It is contrasted to the digital computer, where the calculation is done sequentially.

A microelectromechanical system (MEMS) is a combinatorial system of electric circuits and mechanical systems[24–26]. A typical example is an electrostatic actuator consisting of parallel plates abbreviated as a parallel-plate MEMS. Another important MEMS is a comb-teeth electrostatic actuator abbreviated as a comb-teeth MEMS.

In this paper, we propose an Ising machine with the use of a buckled-plate MEMS made of many parallel plates, which

is a kind of a parallel-plate MEMS. We start with Ising machines simulating a FM interaction and an AF interaction separately. Then, we present a fully-connected MEMS network containing both FM and AF interactions in an arbitrary way. It enables us to solve an arbitrary combinatorial problem described by the Edwards-Anderson model[27], where the FM and AF interactions coexist randomly. The annealing process is shown to be executed automatically due to the damping of the plate motion based on the analytical study of the Euler-Lagrange-Rayleigh equation, where all plates stop once the system reaches a local minimum. We also demonstrate numerically how the annealing actually proceeds. We emphasize that the present Ising machine works at the room temperature without external magnetic field. It is highly contrasted to simulated annealing and quantum annealing, where it is necessary to precisely control external parameters such as temperature and magnetic field.

This paper is composed as follows. In Sec.II we study a buckled-plate MEMS made of many parallel plates, where each plate has two stable positions. In Sec.III, we realize an Ising model by this buckled-plate MEMS with sequential parallel plates to form a chain. We show that the ground state is FM. Buckled plates are manipulated by controlling voltage. We analytically prove that the system reaches a local minimum based on the Euler-Lagrange-Rayleigh formalism. In Sec.IV, we propose an AF Ising model by introducing seesaw structures. In Sec.V, we propose an Ising machine materialized by a fully-connected MEMS network simulating both FM and AF interactions. Sec. VI is devoted to discussion. We prepare Appendices, where we derive various equations used in the main text. We also discuss an Ising model with the use of comb-teeth MEMS by controlling charge.

II. BUCKLED-PLATE MEMS

In the field of MEMS, the bistable structure has been studied with a typical application to memories[28, 29]. We consider a system made of N plates placed parallelly with equal separation, where all plates are buckled as in Fig.1(a). A buckled plate carries the classical bit information $+1$ (-1), when it

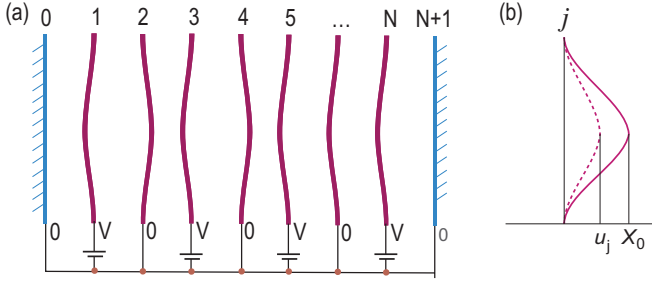


FIG. 1. (a) Illustration of a buckled-plate MEMS, where the direction of buckling is controlled by the electrostatic interaction between the adjacent plates. The voltage at each plate is either 0 or V , alternatively. (b) Enlarged illustration of the j -th buckled plate with the plate position u_j and the stable buckled position X_0 indicated.

is buckled rightward (leftward). All plates are buckled either rightward or leftward in the FM ground state.

The potential energy of the system is well approximated by[30]

$$U_{\text{mech}} = \sum_{j=1}^N \frac{\alpha}{2} (u_j^2 - X_0^2)^2, \quad (1)$$

where α is the strength of the potential, u_j is the position of the j -th plate, and the stable buckled positions are given by $u_j = \pm X_0$, as illustrated in Fig.1(b). The local minima of the potential (1) are given by

$$u_j = \pm X_0. \quad (2)$$

We define the normalized plate position by

$$s_j \equiv u_j / X_0 = \pm 1. \quad (3)$$

The potential barrier is given by

$$U_0 = \frac{\alpha}{2} X_0^4. \quad (4)$$

It is necessary to control a buckled plate between two stable positions.

The simplest is to use an electrostatic interaction between the two adjacent plates as in Fig.1(a). There is another way to use a comb-teeth MEMS between the two adjacent plates, about which we discuss in Appendix F.

In the parallel-plate MEMS, the capacitance between the plate u_j and u_{j+1} is well described by

$$C_{\text{para}}(u_j, u_{j+1}) = \frac{\epsilon_0 S}{X_{\text{cap}} + u_j - u_{j+1}}, \quad (5)$$

where X_{cap} is the distance between the adjacent plates without buckling, S is the area of the plate, and ϵ_0 is the permittivity. The electrostatic potential is given by

$$U_{\text{cap}} = \sum_{j=1}^{N-1} \frac{C_{\text{para}}(u_j, u_{j+1})}{2} V_j^2, \quad (6)$$

when we control the voltage V_j between the j -th and $(j+1)$ -th plates.

The classical bit information ± 1 is carried by the variable u_j , from which the standard bit b_j is defined by

$$u_j = \pm X_0 = (-1)^{s_j} X_0, \quad (7)$$

where $b_j = 0$ or 1. The M -bit state $|b_M b_{M-1} \cdots b_2 b_1\rangle$ is uniquely assigned to the digit state $|N\rangle$, with N being defined by

$$N = \sum_{j=1}^M 2^{j-1} b_j. \quad (8)$$

It is sometimes convenient to use N to represent the M -bit state $|b_M b_{M-1} \cdots b_2 b_1\rangle$.

III. FERROMAGNETIC ISING MODEL

A. Ising model representation

We construct an Ising model by considering the buckled-plate MEMS illustrated in Fig.1(a). The potential energy of the system consists of the mechanical part and the electrostatic part,

$$U_{\text{total}} = U_{\text{mech}} + U_{\text{cap}}, \quad (9)$$

where U_{mech} and U_{cap} are given by Eqs.(1) and (6). Provided the applied voltage V_j is sufficiently smaller than a certain critical value V_{cr} , the ground state is given by Eq.(2), or $s_j = u_j / X_0 = \pm 1$. The critical voltage is given by

$$V_{\text{cr}} = \sqrt{\frac{2\alpha X_0^2 (X_{\text{cap}}^2 - X_0^2)^2}{3\sqrt{3}\epsilon_0 S X_{\text{cap}}}}, \quad (10)$$

as we derive in Appendix B: See Eq.(B5).

Such a binary system is well described by the Ising model. Indeed, it is possible to rewrite the total potential energy (9) in the form of

$$U_{\text{Ising}} = \sum_{j=1}^{N-1} J_j s_j s_{j+1} + E_0, \quad (11)$$

with the use of the system parameters,

$$J_j = -\frac{2\epsilon_0 S V_j^2 X_0^2}{X_{\text{cap}} (X_{\text{cap}}^2 - 4X_0^2)}, \quad (12)$$

and

$$E_0 = \frac{2\epsilon_0 S V_j^2 (X_{\text{cap}}^2 - X_0^2)}{X_{\text{cap}} (X_{\text{cap}}^2 - 4X_0^2)}, \quad (13)$$

as we derive in Appendix: See Eqs.(C23), (C13) and (C15) in Appendix C. The system is FM because J_j is negative definite as in (12).

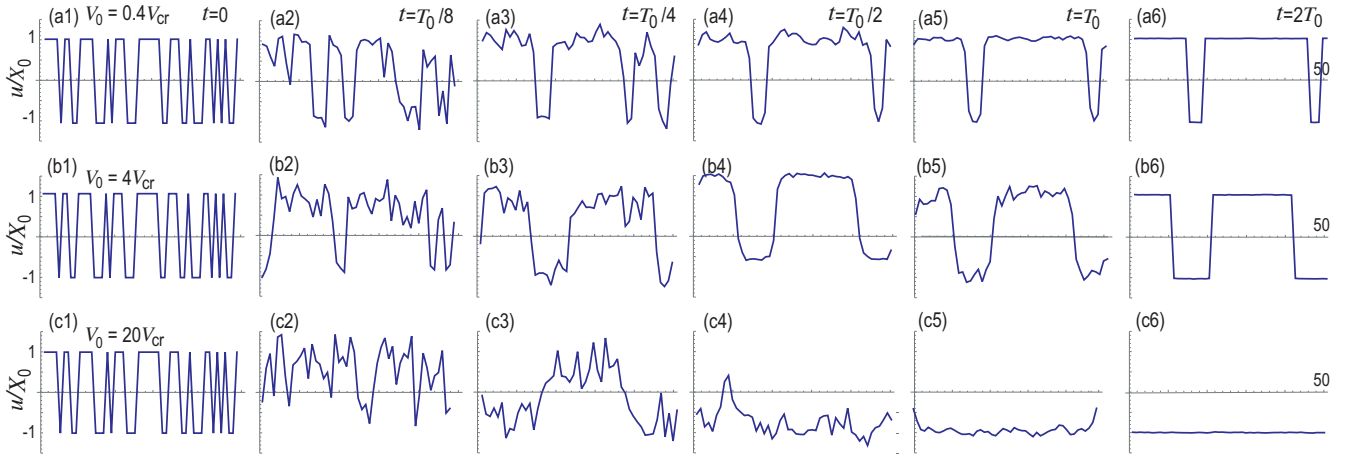


FIG. 2. Dynamics with the fixed-boundary condition. (a1)~(c1) Configuration u_j/X_0 at the initial state $t = 0$; (a2)~(c2) that at $t = T_0/8$; (a3)~(c3) that at $t = T_0/4$; (a4)~(c4) that at $t = T_0/2$; (a5)~(c5) that at $t = T_0$; (a6)~(c6) that at $t = 2T_0$. We have used a 50-plate system. (a1)~(a6) The applied voltage is $V = 0.4V_{cr}$; (b1)~(b6) it is $V = 4V_{cr}$; (c1)~(c6) it is $V = 20V_{cr}$. (a1)~(a6) The applied voltage is $V = 0.4V_{cr}$; (b1)~(b6) it is $V = 4V_{cr}$; (c1)~(c6) it is $V = 20V_{cr}$. (a1)~(a6) There is no annealing when the voltage is below the critical value ($V < V_{cr}$). (b1)~(b6) There remain two domain walls after annealing when the voltage exceeds the critical value but not sufficiently. (c1)~(c6) The annealing process is perfect when the voltage exceeds the critical value sufficiently. The vertical axis is the configuration u_j/X_0 . The horizontal axis is the position j . We have set $\alpha = 0.02$, $\gamma = 0.01$, $T_0 = 500$, $X_0 = 1$, $m = 1$ and $\varepsilon_0 S = 1$.

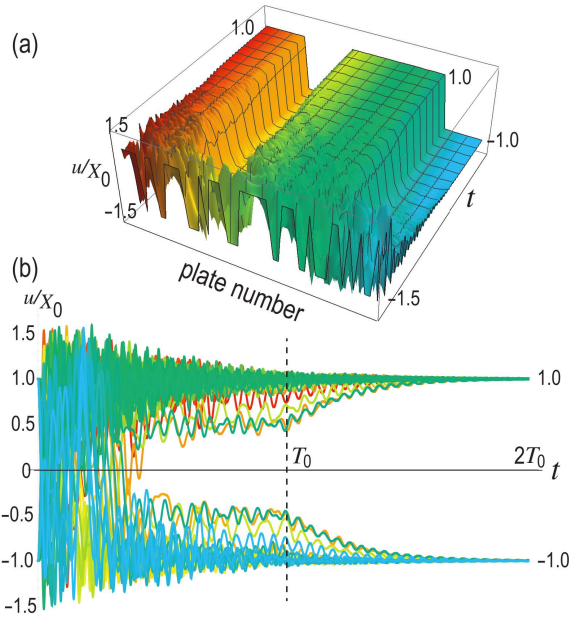


FIG. 3. Time evolution of the annealing process under the fixed-boundary condition, where the exact ground state is achieved as in Fig.2(c6). (a) Bird's eye's view and (b) colored plot for each plate. The vertical axis is the plate position u_j/X_0 . We have used a 50-plate system, and applied $V_0 = 4V_{cr}$. The parameters are the same as in Fig.2. We have used 10^5 time steps for the calculation.

B. Dissipation Mechanism

We start with an initial state, where $s_j = \pm 1$ is randomly assigned to the site j . The configuration is stable without voltage ($V = 0$). We switch on the voltage beyond the critical

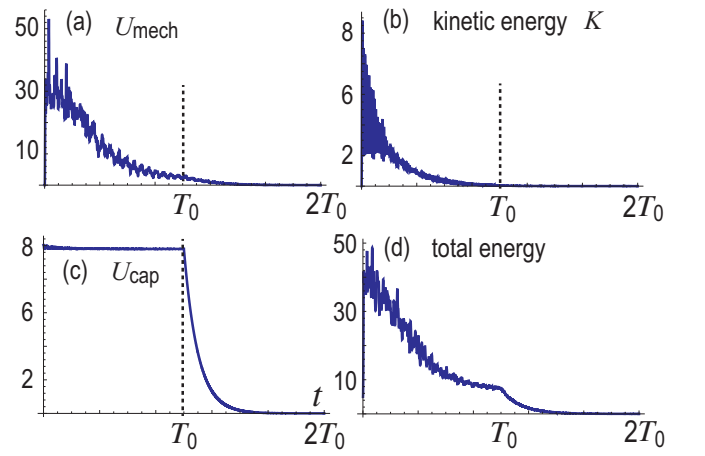


FIG. 4. Time evolution of (a) the mechanical potential energy U_{mech} , (b) the kinetic energy K , (c) the electrostatic potential U_{cap} and (d) total energy under the fixed-boundary condition. We have used a 16-plate system, and applied $V_0 = 20V_{cr}$. The parameters are the same as in Fig.2. The energy is in the unit of $\varepsilon_0 S V_0^2 / X_0$.

value and fix it at $V = V_0$. Then, plates begin to move and the buckling direction may be flipped.

We study the dynamics of the system. The Lagrangian is given by the kinetic term K and the potential (9),

$$L = K - U_{total}, \quad (14)$$

with the kinetic energy

$$K = \sum_j \frac{m}{2} \dot{u}_j^2, \quad (15)$$

where $\dot{u}_j = du_j/dt$ is the velocity of the plate. The Euler-

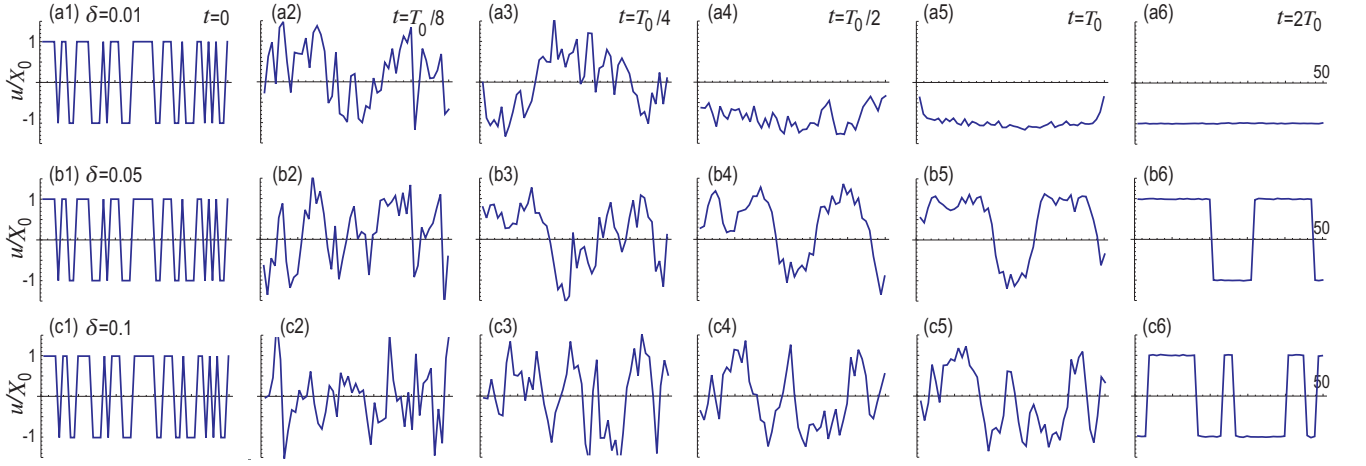


FIG. 5. Dynamics of FM interactions under the fixed-boundary condition in the presence of disorder in X_{cap} . (a1)~(c1) Configuration u_j/X_0 at the initial state $t = 0$, which is taken identical to the one in Fig.2; (a2)~(c2) that at $t = T_0/8$; (a3)~(c3) that at $t = T_0/4$; (a4)~(c4) that at $t = T_0/2$; (a5)~(c5) that at $t = T_0$; (a6)~(c6) that at $t = 2T_0$. (a1)~(a6) The disorder strength is $\delta = 0.01$; (b1)~(b6) it is $\delta = 0.05$; (c1)~(c6) it is $\delta = 0.1$. (a1)~(a6) The annealing process is perfect when the disorder is weak $\delta = 0.01$. (b1)~(b6) There remain three domain walls after annealing when the disorder is medium $\delta = 0.05$. (c1)~(c6) There remain seven domain walls after annealing when the disorder is large $\delta = 0.1$. The vertical axis is the configuration u_j/X_0 , while the horizontal axis is the position of the plate. We have used a 50-plate system, and applied $V = 20V_{\text{cr}}$. We have set $\alpha = 0.02$, $\gamma = 0.01$, $T_0 = 500$ and $X_0 = 10$.

Lagrange-Rayleigh equation is

$$\frac{d}{dt} \left(\frac{\partial L}{\partial \dot{u}_j} \right) - \frac{\partial L}{\partial u_j} + \frac{\partial R}{\partial \dot{u}_j} = 0, \quad (16)$$

where we have introduced the Rayleigh dissipation function in order to describe the damping of the mechanical motion,

$$R = \sum_j \frac{\gamma}{2} \dot{u}_j^2, \quad (17)$$

with γ being the damping factor. Note that the external voltage $V = V_0$ is just a constant.

The total energy is obtained by using the Lagrangian as

$$E \equiv \frac{\partial L}{\partial \dot{u}_j} \dot{u}_j - L. \quad (18)$$

The time dependence of the total energy is given by

$$\frac{dE}{dt} = -\dot{u}_j \frac{\partial R}{\partial \dot{u}_j} = -\sum_j \gamma \dot{u}_j^2, \quad (19)$$

where we have used the relation

$$\begin{aligned} \frac{dL}{dt} &= \dot{q}_i \left(\frac{d}{dt} \frac{\partial L}{\partial \dot{u}_j} + \frac{\partial R}{\partial \dot{u}_j} \right) + \frac{\partial L}{\partial u_j} \dot{u}_j \\ &= \frac{d}{dt} \left(\frac{\partial L}{\partial \dot{u}_j} \dot{u}_j \right) + \dot{u}_j \frac{\partial R}{\partial \dot{u}_j}, \end{aligned} \quad (20)$$

with the aid of the Euler-Lagrange-Rayleigh equation (16). Eq.(19) means that the total energy monotonically decreases as a function of time in the presence of the dissipation term. Eventually, the motion of the plates must stop due to dissipation,

$$\dot{u}_j = 0. \quad (21)$$

This occurs in the presence of the voltage V_0 .

Finally, we decrease adiabatically the voltage to $V = 0$, keeping $\dot{u}_j = 0$. This is a rescaling process, after which a local minimum $u_j = \pm X_0$ or $s_j = \pm 1$ is achieved. This is the basis of the annealing process in the buckled-plate MEMS system based on a dissipation mechanism.

C. Dynamics of plates

We shall demonstrate explicitly how the annealing proceeds and how the plate motion stops to reach a local minimum based on numerical simulations. The dynamics of plates is determined by Eq.(16), which is explicitly written down as

$$\begin{aligned} m\ddot{u}_j + \gamma\dot{u}_j &= -2\alpha u_j (u_j^2 - X_0) - \frac{\varepsilon_0 S V_j^2}{(X_{\text{cap}} + u_j - u_{j+1})^2} \\ &+ \frac{\varepsilon_0 S V_j^2}{(X_{\text{cap}} + u_{j-1} - u_j)^2}. \end{aligned} \quad (22)$$

We solve this equation numerically. We adopt the fixed-boundary condition, where the outmost plates are fixed without buckling as shown in Fig.1(a). The FM ground state is achievable only in this condition. We apply voltage 0 to the $(2n)$ -th plate and V to the $(2n + 1)$ -th plate as shown in Fig.1(a), where the potential difference between two adjacent plates is $\pm V$. We control V according to the formula

$$V = \begin{cases} V_0 & \text{for } t < T_0 \\ V_0 \exp \left[-\frac{t-T_0}{\tau} \right] & \text{for } t \geq T_0 \end{cases}, \quad (23)$$

where τ is the decay rate of the voltage.

First, we set an initial state randomly at the two local minima $s_j = \pm 1$. There are a number of domain walls as in

Fig.2(a1), (b1) and (c1). When V_0 is small enough, the initial state stands as it is. When it overcomes the potential barrier (1) of the buckling, plates begin to move.

Second, we apply a constant voltage V_0 larger than the critical one V_{cr} given in Eq.(10). We show snapshots of the plate positions u_j for three typical values of V_0 in Fig.2. See also Fig.3 for a continuous time evolution in the case of $V_0 = 20V_{cr}$. As the time evolves, the number of domain walls decreases to make the electrostatic energy decrease. We keep the constant voltage $V = V_0$ for a while ($0 < t < T_0$) so that the flipping of plates is completed, as indicated by a vertical dotted line at $t = T_0$ in Fig.3(b). Here, the position u_j deviates from the local minima $u_j = \pm X_0$ because of the presence of V_0 .

The final step is the rescaling process, by adiabatically decreasing the voltage to converge the position u_j to the local minimum $u_j = \pm X_0$ as in Fig.3(b). The FM ground state is achieved when V_0 is taken large enough as in Fig.2(c6).

It is instructive to see the time evolution of various energies. We show the time evolution of the mechanical potential energy (1) in Fig.4(a). It decreases with oscillations but does not reach the zero energy for $t < T_0$, because the relaxed position deviates from the local minima (2) due to the electrostatic force. After the voltage V becomes sufficiently small for $t \gg T_0$, the potential energy goes to zero. On the other hand, the kinetic energy (15) of the plates decreases to zero even for $T < T_0$ due to the Rayleigh dissipation term (17), as shown in Fig.4(b). We also show the time evolution of the electrostatic potential in Fig.4(c). It is almost constant for $T < T_0$ and rapidly decreases for $T > T_0$. The time evolution of the total energy is given in Fig.4(d).

This is the annealing process of the present system. The damping of the mechanical motion plays an essential role in the present annealing process. It is because the total energy automatically decreases due to the damping term, and the plate positions are optimized in this process. It is highly contrasted to the classical and quantum annealing, where it is necessary to gradually decrease temperature or magnetic field due to the lack of dissipation mechanism.

D. Effect of randomness

Next, we study effects of randomness. We introduce randomness into the plate distance X_{cap} uniformly distributing from $-\delta$ to δ . Then, the distance X_{cap} becomes node-dependent, $X_{cap} \rightarrow X_{cap,n}$, where

$$X_{cap,n} = X_{cap} (1 + \eta_n \delta), \quad (24)$$

with η_n being a random variable ranging from -1 to 1 . We show the time evolution of the plate positions u_j by applying $V_0 = 20V_{cr}$ in Fig.5. When the disorder strength is not too large, the annealing process is perfectly executed as shown in Fig.5(a6). Hence, it is necessary to make a sample where the disorder is smaller than $\delta = 0.01$ in order to execute annealing process. We comment that the presence of randomness is not serious since it is remedied by introducing additional springs

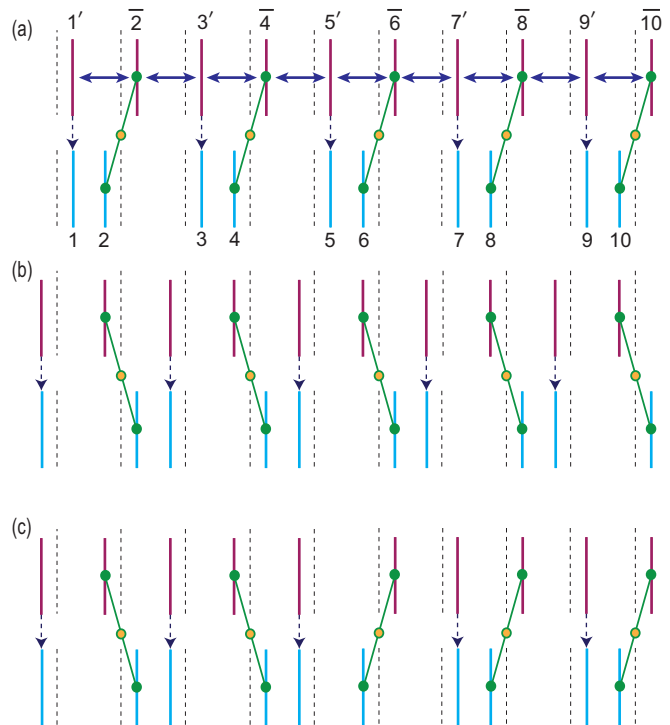


FIG. 6. Illustration of a MEMS realizing AF interactions. (a) This is a ground state representing an AF configuration in the lower chain. Double-headed arrows represent electrostatic interactions. (b) This is the other AF ground state. The ground states are two-fold degenerate. (c) An example of excited states, containing one domain wall. Purple plates are metallic plates and move dynamically by electrostatic interactions, while cyan plates are plastic plates representing the original bit b_j . There are two types of purple plates: One is connected to a cyan plate by a seesaw, representing the inverted bit \bar{b}_j ; the other is connected to a cyan plate without a seesaw, representing the copied bit b'_j . The cyan plate indexed by the original bit b_j moves in the forward (reverse) direction of the paired purple plate indexed by the copied bit b'_j (inverted bit \bar{b}_j). The AF order is realized for the original bits in the lower chain in this way.

to the buckled-MEMS, about which we discuss in Appendix C.

IV. ANTIFERROMAGNETIC ISING MODEL

In the above construction, only the FM interactions are realized. However, AF interactions are also necessary in order to solve nontrivial Ising problems. We propose a seesaw mechanism shown in Fig.6(a), where an even-numbered plate (in purple) in the upper chain is connected to a plate (in cyan) in the lower chain by a spring (in green) rotating around an fixed point (in orange). These two plates move simultaneously preserving the condition

$$u_j \equiv (-1)^j u_j^{\text{lower}}. \quad (25)$$

On the other hand, an odd-numbered plate (in purple) in the upper chain moves precisely in the same way as a plate (in

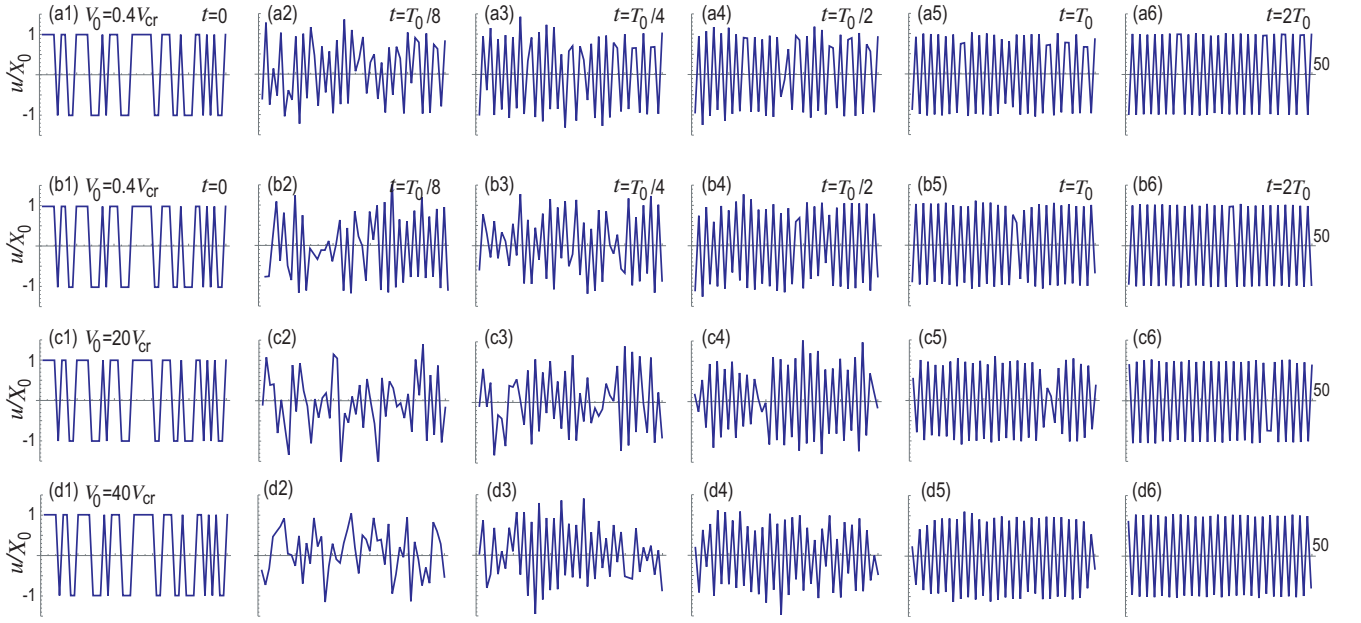


FIG. 7. Dynamics of AF interactions with the fixed-boundary condition. (a1)~(c1) Configuration u_j/X_0 at the initial state $t = 0$; (a2)~(c2) that at $t = T_0/8$; (a3)~(c3) that at $t = T_0/4$; (a4)~(c4) that at $t = T_0/2$; (a5)~(c5) that at $t = T_0$; (a6)~(c6) that at $t = 2T_0$. We have used a 50-plate system. (a1)~(a6) The applied voltage is $V = 0.4V_{cr}$; (b1)~(b6) it is $V = 4V_{cr}$; (c1)~(c6) it is $V = 20V_{cr}$ and (d1)~(d6) it is $V = 40V_{cr}$. (a1)~(a6) There is no annealing when the voltage is below the critical value ($V < V_{cr}$). (b1)~(b6) and (c1)~(c6) There remain some domain walls after annealing when the voltage exceeds the critical value but not sufficiently. (d1)~(d6) The annealing process is perfect when the voltage exceeds the critical value sufficiently. The vertical axis is the configuration u_j/X_0 . The horizontal axis is the position j . We have set $\alpha = 0.02$, $\gamma = 0.01$, $T_0 = 500$ and $X_0 = 10$.

cyan) in the lower chain. The electrostatic interaction operates between the adjacent plates only in the upper chain. Plates in the lower chain are made of nonmetallic material such as plastic and gum, and are not components of MEMS.

When the bit b_j assigned in the lower chain and the bit \bar{b}_j in the upper chain are connected by a seesaw, the condition (25) introduces the relation between them,

$$\bar{0}_j = 1_j, \quad \bar{1}_j = 0_j. \quad (26)$$

The barred bit is called the inverted bit. On the other hand, when they are not connected by a seesaw, the bits are identical between the two chains,

$$b'_j = b_j. \quad (27)$$

The dashed bit is called the copied bit.

We now argue that the AF Ising model is realized in the lower chain in Fig.6. By inserting Eq.(25) to the Hamiltonian (C5), we obtain the Hamiltonian

$$H_j(s_j, s_{j+1}) = -J_j s_j s_{j+1} + \frac{B_j}{2} (-1)^j s_j + \frac{B_{j+1}}{2} (-1)^{j+1} s_{j+1} + \frac{E_0}{N-1}, \quad (28)$$

which represents the AF Ising model. The electrostatic potential is represented as

$$U_{cap} = \sum_{j=1}^{N-1} \frac{C_{para}((-1)^j u_j, (-1)^{j+1} u_{j+1})}{2} V_j^2, \quad (29)$$

in terms of the position u_j of the plate in the lower chain, where the use was made of Eq.(25). By inserting it to the Euler-Lagrange-Rayleigh equation (16), we obtain the equations of motion for the lower chain

$$m(-1)^j \ddot{u}_j + \gamma(-1)^j \dot{u}_j = -2\beta(-1)^j u_j (u_j^2 - X_0) - \frac{\varepsilon_0 S V_j^2}{(X_{cap} + (-1)^j u_j - (-1)^{j+1} u_{j+1})^2} + \frac{\varepsilon_0 S V_j^2}{(X_{cap} + (-1)^{j-1} u_{j-1} - (-1)^j u_j)^2}. \quad (30)$$

We show numerical results of the dynamics in the configuration in Fig.7 for various applied constant voltage V_0 . When we apply a weak voltage, there is almost no annealing and there are many domain walls as in Fig.7(a6). When we apply a medium voltage, the annealing process is not sufficient and the final state have AF domain walls in an instance of Fig.7(b6) and (c6). When we apply a strong voltage, the final state is perfectly antiferromagnet as an instance of Fig.7(d6). These results show that AF interactions are well simulated by using the seesaw configuration shown in Fig.6.

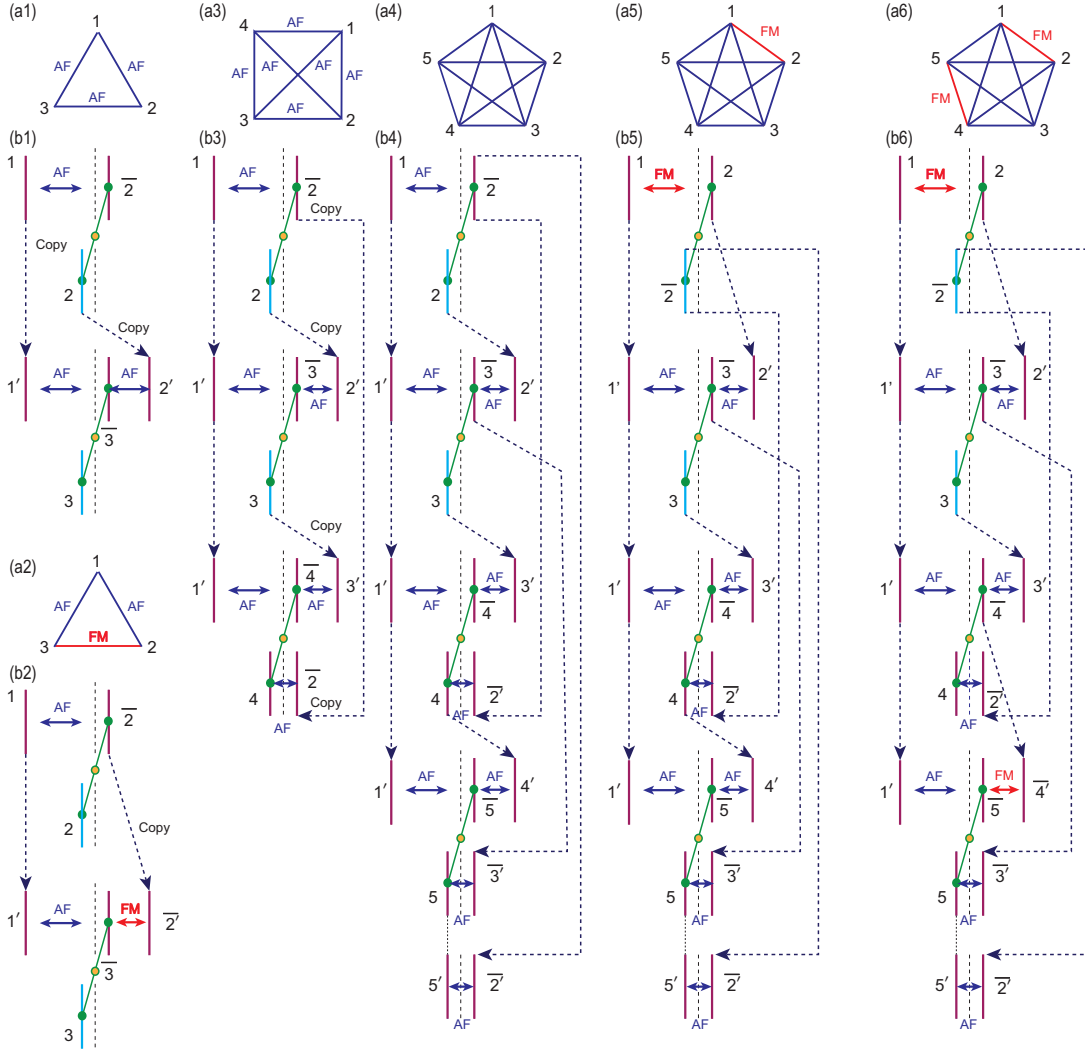


FIG. 8. (a) Illustration of fully-connected bits. Ferromagnetic interactions are marked in red lines and AF interactions are marked in blue lines. (a1) Fully-connected three bits with AF interactions. (a2) Fully-connected three bits with two AF and one FM interactions. (a3) Fully-connected four bits with AF interactions. (a4) Fully-connected five bits with AF interactions. (a5) Fully-connected five bits with AF interactions except for one FM interaction. (a6) Fully-connected five bits with AF interactions except for two FM interactions. (b1)~(b6) Illustration of a fully-connected buckled-plate MEMS. Effective electrostatic interactions are indicated by double-headed arrows between two purple plates. The number in the vicinity of a plate indicates the number of a bit. A pair of plates connected by a dotted arrow are indexed by the original bit b_j and the copied bit b'_j , and they move simultaneously. A pair of plates connected by a seesaw are indexed by the original bit b_j and the inverted bit \bar{b}_j , and they move inversely.

V. FULLY-CONNECTED ANNEALING MACHINE

In order to solve a nontrivial problem, it is necessary to construct a fully-connected system, where both FM and AF interactions coexist. It looks that it is almost impossible to construct a fully-connected system because we need $(M - 1)$ plates interacting electrostatically with one plate in the present buckled-plate MEMS configuration. However, it has been proposed in the context of quantum annealing machines that the fully-connected system can be constructed by introducing copied bits[31, 32].

We use this idea in the MEMS annealing machine as illustrated in Fig.8. We prepare a copy of a plate in such a way

that the motion is identical to the original plate. We denote the copied bit of the original bit b_j by b'_j . It is materialized by bridging two plates, where we adjust that the total mass of the original and copied bits is identical. It is always possible because the original and copied bit form a rigid body. Then, we introduce an electrostatic interaction between an original plate and a copied plate. By adding an appropriate number of copied plates, it is possible to materialize a fully-connected system. Furthermore, it is possible to materialize a fully-connected system containing both FM and AF interactions in a single network by appropriately choosing the position of interactions.

We note that the interaction is FM between b_j and b_k , be-

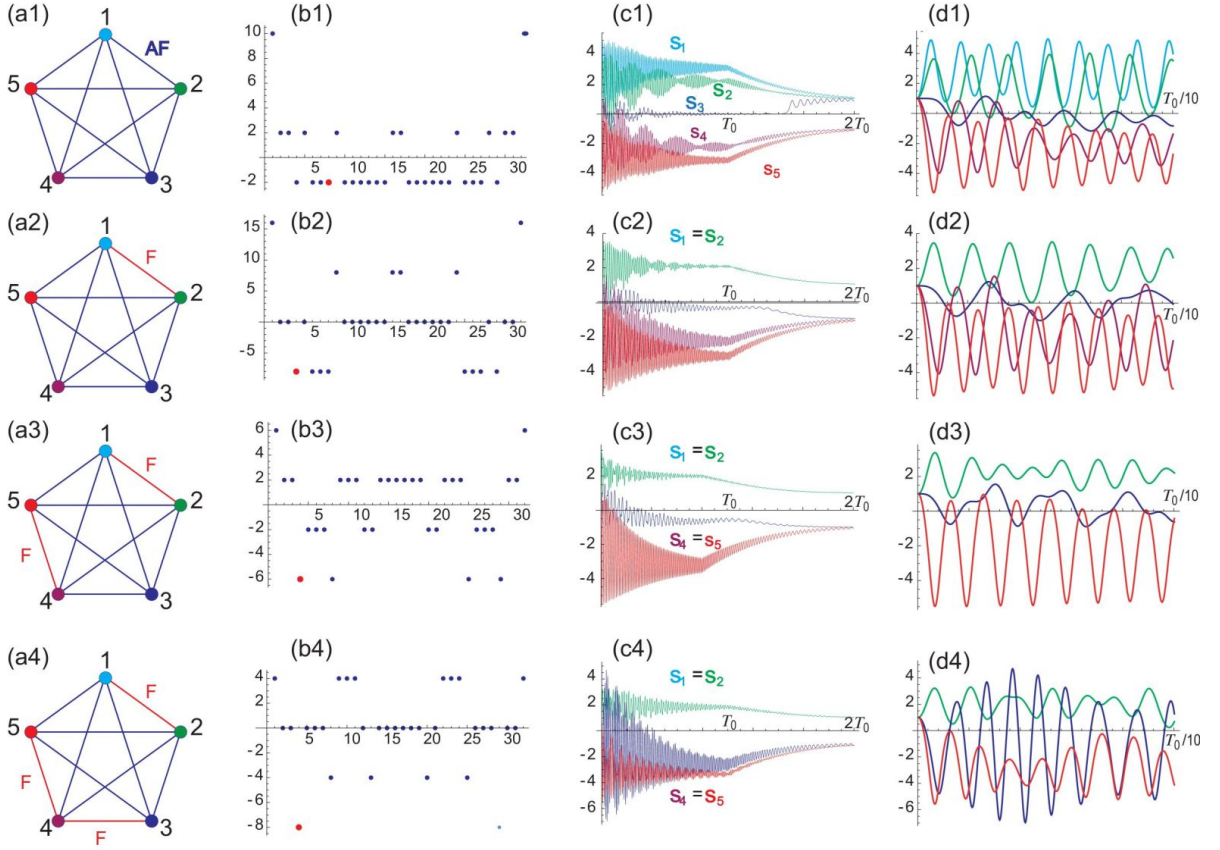


FIG. 9. (a) Illustration of fully-connected five bits, which are the same as in Fig.8(a). (b) The energy spectrum as a function of the digit state $|N\rangle$ defined by Eq.(8). The numerical results are marked in red, which is one of the degenerated ground states. When we start from the initial state $|00000\rangle = |0\rangle$, one of the ground state $|00111\rangle = |7\rangle$ is chosen in (b1), while $|00011\rangle = |3\rangle$ is chosen in (b2), (b3) and (b4) by the annealing process. The vertical axis is the energy in units of J . (c) Time evolution of the annealing process for $0 \leq t \leq 2T_0$, where the vertical axis stands for the normalized plate position s_j . The first normalized plate position s_1 is indicated by cyan curve, the second one s_2 by green curve, the third one s_3 by blue curve, the fourth one s_4 by purple curve and the fifth one s_5 by red curve. We have set $\alpha = 0.02$, $\gamma = 0.01$, $T_0 = 500$ and $X_0 = 10$. (d) Initial time evolution of the annealing process for $0 \leq t \leq 0.1T_0 = 50$, where the vertical axis is u_j . We have applied $V = 40V_{cr}$.

tween b'_j and b_k , and between b'_j and b'_k . It is also FM between \bar{b}_j and \bar{b}_k , and so on. On the other hand, the interaction is AF between b_j and \bar{b}_k , and so on.

We present how to construct the MEMS annealing machine by taking an instance of the three-bit fully-connected AF system in Fig.8(a1). (i) We introduce an AF interaction between the bit 1 and the inverted bit $\bar{2}$ as in the case of the left-most two bits in Fig.6. (ii) In the same way, we introduce an AF interaction between the bit 1 and the inverted bit $\bar{3}$. (iii) As the final step, we introduce an AF interaction between the copied bit $2'$ and the inverted bit $\bar{3}$ as in Fig.8(b1).

The next instance is the three-bit fully-connected AF and FM system shown in Fig.8(a2). The first two steps (i) and (ii) are identical. Only the final step (iii) is different, in which we introduce an FM interaction between the inverted copied bit $\bar{2}'$ and the inverted bit $\bar{3}$ as in Fig.8(b2).

This method is applicable to any fully-connected network. In the M -bit system, we introduce $M - 1$ AF links starting from the bit 1 by introducing $M - 2$ copied bits $1'$. Then, we introduce an AF or FM link between any pair of bits except the

bit 1 by introducing necessary copied bits. Explicit examples are given in Figs.8(b3)~(b6) for $M = 4$ and 5.

For the FM interaction between j and k , the equations of motion are given by

$$\begin{aligned} m\ddot{u}_j + \gamma\dot{u}_j + 2\alpha u_j (u_j^2 - X_0) &= -\frac{\varepsilon_0 S V_{jk}^2}{(X_{cap} + u_j - u_k)^2}, \\ m\ddot{u}_k + \gamma\dot{u}_k + 2\alpha u_k (u_k^2 - X_0) &= -\frac{\varepsilon_0 S V_{jk}^2}{(X_{cap} + u_k - u_j)^2}. \end{aligned} \quad (31)$$

On the other hand, the AF interaction between j and k , the equations of motion are given by

$$\begin{aligned} m\ddot{u}_j + \gamma\dot{u}_j + 2\alpha u_j (u_j^2 - X_0) &= \frac{\varepsilon_0 S V_{jk}^2}{(X_{cap} + u_j - u_k)^2}, \\ m\ddot{u}_k + \gamma\dot{u}_k + 2\alpha u_k (u_k^2 - X_0) &= -\frac{\varepsilon_0 S V_{jk}^2}{(X_{cap} + u_j - u_k)^2}. \end{aligned} \quad (32)$$

More detailed equations are given in Appendix G.

We present numerical results for five-bit fully-connected networks in Figs.9(a1)~(a4). The energy spectrum is shown in Figs.8(b1)~(b4) as a function of the digit state $|N\rangle$ representing the 5 bits $|b_5b_4b_3b_2b_1\rangle$: See Eq.(8). For example, the energy spectrum for this system is shown in Fig.9(b1), where more than half of states form the degenerated ground states. In Fig.8(a5), one AF interaction is replaced by a FM interaction. The corresponding energy spectrum is shown in Fig.9(b2), where the degeneracy becomes smaller than the totally AF system. The dynamics are identical between the bit 1 and the bit 2, which would be due to the introduction of the FM interactions between the bit 1 and the bit 2 as shown in Fig.9(c2). A further introduction of the FM interactions as shown in Fig.8(a6) leads to a further decrease of the degeneracy of the ground states as shown in Fig.9(b4). The dynamics are identical between the bit 4 and bit 5 in addition to the bit 1 and the bit 2, which would be due to the introduction of the FM interactions between the bit 4 and the bit 5 as shown in Fig.9(c3). When there are three FM interactions as in Fig.9(a4), there are only two-fold degenerate ground states as shown in Fig.9(b4). Nevertheless, one of the ground states is correctly obtained as in Fig.9(c4).

In Fig.9(c), the numerically solved annealing process for the 5 qubit system is presented, where we start with the initial condition $|00000\rangle = |0\rangle$. We find that the exact ground state is reached by the annealing process for various systems. In all cases, the obtained ground state is $|00111\rangle = |7\rangle$ for Fig.9(b1) and $|00011\rangle = |3\rangle$ for Fig.9(b2)~(b4). It indicates that the present MEMS annealing machine can solve arbitrary nontrivial problems.

VI. DISCUSSIONS

We have proposed an application of MEMS to an Ising machine. In order to solve nontrivial Ising problems, it is necessary to construct the Edwards-Anderson model[27], where the FM and AF interactions coexist arbitrarily. We have proposed a method to construct a mechanism solving such a problem with the aid of a fully-connected MEMS network.

We have used the buckled-plate MEMS to explain an Ising machine for its simplicity. Actually, to avoid the pull-in instability, an Ising machine based on the comb-teeth MEMS would be better, about with we discuss in Appendix G. The comb-teeth MEMS looks a bit complicated but its fabrication is possible in the present technology. The translation of mathematical formulas is simple between these two types of MEMS because there holds a duality relation between them, as we explain in Appendix G.

We comment that there is another proposal on the Ising machine based on MEMS[33], where bistable vibrations are used based on the parametric resonances of multiple modes. It presents a different realization of the MEMS Ising machine from the present proposal.

In general, temperature is controlled in classical annealing, while external magnetic field is controlled in quantum annealing. They are set above the critical values in the initial stage.

Then, they are gradually decreased, during which the annealing proceeds. On the other hand, we control external voltage in the annealing method based on the buckled-plate MEMS. In the first step of the annealing process, we keep a constant voltage for a certain period. The essential part of the annealing is completed due to the Rayleigh dissipation term. Although we gradually decrease the voltage, this is just to rescale the position to $u_j = \pm X_0$. Thus, the annealing process is quite different from the standard ones. We would like to point out that the control of the voltage is easier than the control of the temperature or the magnetic field, which will be of benefit to future applications. In addition, our mechanism works at the room temperature without applying external magnetic field.

The speed and energy consumption depend on the size of MEMS. In general, the speed is higher and the energy consumption is lower if the size of MEMS is smaller. The flipping speed is around 1kHz in standard MEMS. In the annealing process shown in Fig.2, the number of flips are of the order of one thousand times, which requires one second. In this context, it is better to construct an annealing machine in Nano-Electro-Mechanical System (NEMS). See Appendix D for the characteristic frequency.

The speed of our annealing machine based on MEMS may not depend on the number of the plates because the plates move simultaneously to minimize the energy. It is contrasted to the digital simulations, where the calculation is done sequentially in a software model. The speed may be much faster in the MEMS machine when the number of plates is large. It is a merit of a machine based on the rules of nature in the spirit of Feynman's idea[23] as pointed out in Introduction.

In passing, we would like to report that we have already fabricated some basic elements of the present MEMS Ising machine[34, 35] after submission of this paper.

M. E. is very much grateful to E. Saito and N. Nagaosa for helpful discussions on the subject. Y. M. is supported by CREST, JST (JPMJCR20T2). M. E. is supported by the Grants-in-Aid for Scientific Research from MEXT KAKENHI (Grants No. JP17K05490 and No. JP18H03676) and CREST, JST (JPMJCR16F1 and JPMJCR20T2).

Appendix A: MEMS memory

Before we derive the critical voltage of the MEMS Ising machine, i.e., Eq.(10) in the main text, we analyze a similar but simpler system, that is a MEMS memory[30] consisting of three plates as shown in Fig.10. The outermost two plates are fixed at the position $u_1 = u_3 = 0$, while the inner plate $u \equiv u_2$ can move freely. There are two stable positions $u = \pm X_0$, which can store a binary information. The position of the plate can be read out by measuring the capacitance. This can be used as a binary memory.

We discuss how to flip the stored information. We choose the initial state $u = -X_0$, as shown in Fig.10(a). We apply a voltage between the right and middle plates as shown in Fig.10(b). The electrostatic potential is given by

$$C_{\text{para}}(u) = \frac{\varepsilon_0 S}{X_{\text{cap}} + u}. \quad (\text{A1})$$

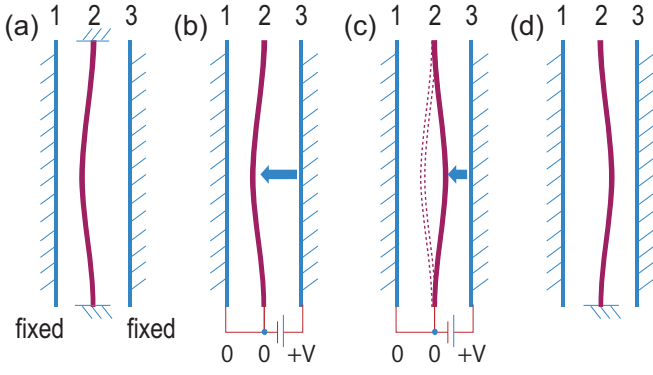


FIG. 10. Flip process of the MEMS memory. (a) The initial position of the plate is $u = -X_0$. (b) We apply voltage between the central and the right plates. (c) The position is flipped from $u = -X_0$ to $u = X_0$. (d) We remove the voltage, where the plate is fixed at $u = X_0$.

The static energy is given by

$$U_{\text{cap}} = \frac{C_{\text{para}}(u)}{2} V^2, \quad (\text{A2})$$

when we apply a constant voltage V between the right and middle plates.

The position u is determined by the total potential,

$$U_{\text{total}}(u) = \frac{\alpha}{2} (u^2 - X_0^2)^2 + \frac{C_{\text{para}}(u)}{2} V^2. \quad (\text{A3})$$

We analyze the condition for the central plate to move from the left position to the right position without a barrier: See Fig.10(c) and Fig.11. The condition is that the slope of the curve $U_{\text{total}}(u)$ is negative, $\partial U_{\text{total}}/\partial u < 0$, for all $|u| < X_0$. In order to solve this condition, we determine a position u_0 where the slope of $\partial U_{\text{total}}/\partial u$ is zero, or

$$\left. \frac{\partial^2 U_{\text{total}}}{\partial u^2} \right|_{u_0} = 0. \quad (\text{A4})$$

If the condition

$$\left. \frac{\partial U_{\text{total}}}{\partial u} \right|_{u_0} < 0 \quad (\text{A5})$$

is satisfied at this position $u = u_0$, it follows that $\partial U_{\text{total}}/\partial u < 0$ for $u < X_0$. See Fig.11(c2).

By using an approximation $X_{\text{cap}} \gg u$, the static energy is approximated as

$$U_{\text{cap}} \simeq \frac{\varepsilon_0 S V^2}{2 X_{\text{cap}}} \left(1 - \frac{u}{X_{\text{cap}}} \right). \quad (\text{A6})$$

By inserting it to Eq.(A3) and Eq.(A4), we find

$$\frac{\partial^2 U_{\text{total}}}{\partial u^2} = 4\alpha u^2 + 2\alpha (u^2 - X_0^2) = 0, \quad (\text{A7})$$

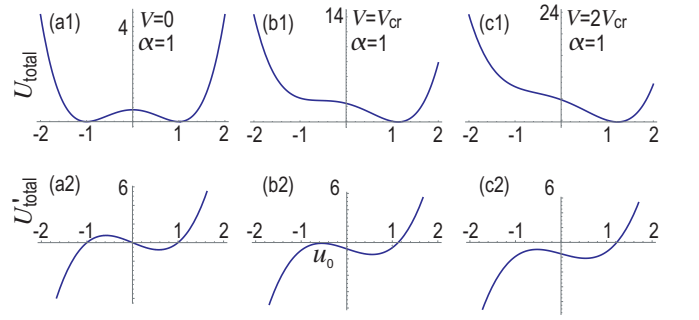


FIG. 11. (a1) Total potential U_{total} with $V = 0$ (i.e., the mechanical potential U_{mech}) for three plates given by Fig.10, where $u_1 = u_3 = 0$. (b1) U_{total} with $V = V_{\text{cr}}$. (c1) U_{total} with $V > V_{\text{cr}}$. (a2), (b2) and (c2) corresponding differential of the potential $U'_{\text{total}} = \partial U_{\text{total}}/\partial u$. We have set $\alpha = 1$. The horizontal axis is the position in units of X_0 .

whose solution is $u_0 = -X_0/\sqrt{3}$. Now, the condition (A5) yields

$$\begin{aligned} \left. \frac{\partial U_{\text{total}}}{\partial u} \right|_{u_0} &= 2\alpha u (u^2 - X_0^2) - \frac{\varepsilon_0 S}{2 X_{\text{cap}}^2} V^2 \Big|_{u_0} \\ &= \frac{4\alpha X_0^3}{3\sqrt{3}} - \frac{\varepsilon_0 S}{2 X_{\text{cap}}^2} V^2 < 0, \end{aligned} \quad (\text{A8})$$

from which we obtain $V > V_{\text{cr}}$ with

$$V_{\text{cr}} = \sqrt{\frac{8\alpha X_0^3 X_{\text{cap}}^2}{3\sqrt{3}\varepsilon_0 S}}. \quad (\text{A9})$$

The plate position flips from $u = -X_0$ to $u = X_0$ for $V > V_{\text{cr}}$. Finally, we remove the voltage, where the plate is fixed at $u = X_0$, as shown in Fig.10(d).

Appendix B: Flipping dynamics

The flipping dynamics of the MEMS Ising machine can be understood intuitively by plotting the potential $U_{\text{total}} = U_{\text{mech}} + U_{\text{cap}}$. For simplicity, we first consider three plates, where two outermost plates are fixed at the position $u_1 = u_3 = X_0$ while the inner plate moves freely. The electrostatic potential is given by

$$U_{\text{cap}} = \frac{\varepsilon_0 S}{X_{\text{cap}} - u + X_0} + \frac{\varepsilon_0 S}{X_{\text{cap}} - X_0 + u}. \quad (\text{B1})$$

We show the electrostatic potential as a function of the position of the inner plate u in Fig.12(b). It takes a minimum at $u = X_0$, which indicates that the inner plate tends to take the same position as the outermost plates. There are two minima in the spring potential energy as shown in Fig.12(a). By increasing the voltage, the energy balance is broken. Fig.12(c) shows a potential with a critical voltage. Once, the voltage exceeds the critical point, the potential has only one minimum without energy barrier as shown in Fig.12(d). Then, the inner plate moves so that the position u is identical to the positions

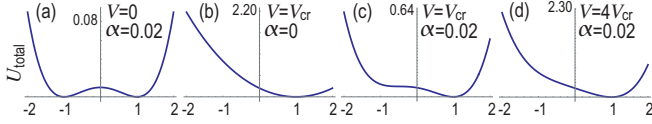


FIG. 12. Total potential energy U_{total} . (a) Spring potential (1) with $\alpha = 0.02$. (b) Electrostatic potential (6) with $\alpha = 0$ and $V = V_{\text{cr}}$. (c) $\alpha = 0.02$ and $V = V_{\text{cr}}$. (d) $\alpha = 0.02$ and $V = 4V_{\text{cr}}$.

of the outermost plates, i.e., $u = u_1 = u_3 = X_0$. It corresponds to the FM interaction in the Ising model.

We derive the critical voltage as in the case of the MEMS memory. By using an approximation $X_{\text{cap}} \gg u$, the static energy is approximated as

$$U_{\text{cap}} \simeq \frac{\varepsilon_0 S V^2 X_{\text{cap}}}{2 (X_{\text{cap}}^2 - X_0^2)} \left(1 - \frac{2X_0}{X_{\text{cap}}^2 - X_0^2} u \right). \quad (\text{B2})$$

The stationary solution u_0 is obtained by solving Eq.(A4), or

$$\frac{\partial^2 U_{\text{total}}}{\partial u^2} = 4\alpha u^2 + 2\alpha (u^2 - X_0^2) = 0. \quad (\text{B3})$$

It yields $u_0 = -X_0/\sqrt{3}$. Then, the critical value is obtained from (A5), or

$$\begin{aligned} \left. \frac{\partial U_{\text{total}}}{\partial u} \right|_{u_0} &= 2\alpha u (u^2 - X_0^2) - \frac{2\varepsilon_0 S X_{\text{cap}} X_0}{(X_{\text{cap}}^2 - X_0^2)^2} V^2 \Big|_{u_0} \\ &= \frac{4\alpha X_0^3}{3\sqrt{3}} - \frac{2\varepsilon_0 S X_{\text{cap}} X_0}{(X_{\text{cap}}^2 - X_0^2)^2} V^2 < 0. \end{aligned} \quad (\text{B4})$$

It yields $V > V_{\text{cr}}$ with

$$V_{\text{cr}} = \sqrt{\frac{2\alpha X_0^2 (X_{\text{cap}}^2 - X_0^2)^2}{3\sqrt{3}\varepsilon_0 S X_{\text{cap}}}}. \quad (\text{B5})$$

This is Eq.(10) in the main text. It is necessary to apply a voltage larger than the critical voltage V_{cr} in order to carry out the MEMS computing.

Appendix C: Derivation of Ising model

The potential energy of the buckled-plate MEMS is given by

$$U_{\text{total}} = U_{\text{mech}} + U_{\text{cap}}, \quad (\text{C1})$$

where U_{mech} is given by Eq.(1) and

$$U_{\text{cap}} = \sum_{j=1}^{N-1} \frac{C_{\text{para}}(u_j, u_{j+1})}{2} V_j^2. \quad (\text{C2})$$

Provided the applied voltage V_j is sufficiently smaller than V_{cr} , the ground state is given by Eq.(2), or $s_j \equiv u_j/X_0 = \pm 1$.

We show that the potential energy (C1) may be written in the form of the Ising model under external field B_j ,

$$H_{\text{Ising}} = \sum_{j=1}^{N-1} J_j s_j s_{j+1} + \sum_{j=1}^N B_j s_j + E_0. \quad (\text{C3})$$

We rewrite Eq.(C3) as

$$H_{\text{Ising}} = \sum_{j=1}^{N-1} H_j (s_j, s_{j+1}) + \frac{B_1}{2} s_1 + \frac{B_N}{2} s_N, \quad (\text{C4})$$

with

$$H_j (s_j, s_{j+1}) = J_j s_j s_{j+1} + \frac{B_j}{2} s_j + \frac{B_{j+1}}{2} s_{j+1} + \frac{E_0}{N-1}. \quad (\text{C5})$$

We realize the term (C5) by a system made of two adjacent buckled plates j and $j+1$.

The energy $H_j (s_j, s_{j+1})$ of the Ising Hamiltonian is given by setting $s_j = \pm 1$ in Eq.(C5), while the energy U_{cap} of the buckled-plate MEMS is given by setting $u_j = X_0 s_j$ in Eq.(C2) provided $V/V_{\text{cr}} \ll 1$. By identifying them, we obtain a formula

$$H_j (s_j, s_{j+1}) = \frac{C_{\text{para}}(u_j, u_{j+1})}{2} V_j^2 \quad (\text{C6})$$

with $u_j = X_0 s_j$ under the constant-voltage condition. Note that we have $U_{\text{mech}} = 0$ since the plates exist at the stable position. The condition (C6) determines the parameters J_j , B_j and E_0 in Eq.(C3).

We write down $H_{j,j+1} (s_j, s_{j+1})$ explicitly,

$$H_j (1, 1) = J_j + B'_j + B'_{j+1} + E'_0 \equiv \mathcal{E}_0, \quad (\text{C7})$$

$$H_j (1, -1) = -J_j + B'_j - B'_{j+1} + E'_0 \equiv \mathcal{E}_+, \quad (\text{C8})$$

$$H_j (-1, 1) = -J_j - B'_j + B'_{j+1} + E'_0 \equiv \mathcal{E}_-, \quad (\text{C9})$$

$$H_j (-1, -1) = J_j - B'_j - B'_{j+1} + E'_0 \equiv \mathcal{E}_0, \quad (\text{C10})$$

where we have defined $B'_j = B_j/2$ and $E'_0 = E_0/(N-1)$. It follows from Eqs.(C6) and (5) that

$$\mathcal{E}_0 = \frac{\varepsilon_0 S}{X_{\text{cap}} - X_0 + X_0} \frac{V_j^2}{2} = \frac{\varepsilon_0 S}{X_{\text{cap}}} \frac{V_j^2}{2}, \quad (\text{C11})$$

$$\mathcal{E}_{\pm} = \frac{\varepsilon_0 S}{X_{\text{cap}} \mp X_0 \mp X_0} \frac{V_j^2}{2} = \frac{\varepsilon_0 S}{X_{\text{cap}} \mp 2X_0} \frac{V_j^2}{2}. \quad (\text{C12})$$

We find $\mathcal{E}_+ > \mathcal{E}_0 > \mathcal{E}_-$. Hence, the coefficients in the Ising model are given

$$J_j = \frac{2\mathcal{E}_0 - \mathcal{E}_+ - \mathcal{E}_-}{4} = -\frac{2\varepsilon_0 S V_j^2 X_0^2}{X_{\text{cap}} (X_{\text{cap}}^2 - 4X_0^2)}, \quad (\text{C13})$$

$$B_j = -B_{j+1} = \frac{\mathcal{E}_+ - \mathcal{E}_-}{4} = \frac{\varepsilon_0 S V_j^2 X_0}{(X_{\text{cap}}^2 - 4X_0^2)}, \quad (\text{C14})$$

$$E_0 = \frac{2\mathcal{E}_0 + \mathcal{E}_+ + \mathcal{E}_-}{4} = \frac{2\varepsilon_0 S V_j^2 (X_{\text{cap}}^2 - X_0^2)}{X_{\text{cap}} (X_{\text{cap}}^2 - 4X_0^2)}, \quad (\text{C15})$$

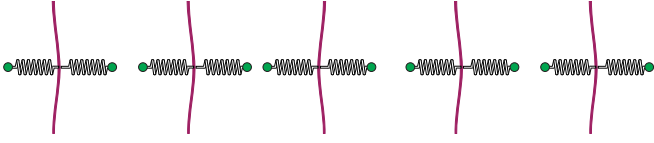


FIG. 13. Illustration of plates connected by springs. Each buckled plate is connected by a spring where the other end is fixed. This structure realizes the pure Ising model without external field term $B_j s_j$.

in terms of the quantities of the buckled-plate MEMS.

We recall that we apply a constant voltage V at the odd plates while the odd plates are grounded in the Ising machine. Then, the voltage is given by $V_{2j-1} = -V$ and $V_{2j} = V$. See Fig.1(a). It results in the constant voltage $V_j^2 = V^2$. The Hamiltonian (C3) is reduced to

$$H_{\text{Ising}} = \sum_{j=1}^{N-1} J_j s_j s_{j+1} + B_1 s_1 + B_N s_N + E_0, \quad (\text{C16})$$

since the $B_j s_j$ terms cancel except for the end plates. Here, J_j , $B_1 = -B_N$ and E_0 are given by Eqs.(C13), (C14) and (C15), respectively.

However, X_{cap} is inhomogeneous in the presence of randomness, where the $B_j s_j$ terms do not cancel. In order to control the $B_j s_j$ term independently, we introduce an additional spring connecting a plate and a fixed point as in Fig.13, leading to the potential energy given by

$$U_{\text{add}} = \frac{\kappa}{2} \sum_{j=1}^N (u_j - X_j^{\text{add}})^2. \quad (\text{C17})$$

The modified Ising Hamiltonian is

$$H'_{\text{Ising}} = H_{\text{Ising}} + \sum_{j=1}^N H_{\text{add}}(s_j), \quad (\text{C18})$$

with

$$\begin{aligned} H_{\text{add}}(s_j) &= \frac{\kappa}{2} (s_j X_0 - X_j^{\text{add}})^2 \\ &= \kappa X_0 X_j^{\text{add}} s_j + \frac{\kappa}{2} (X_0^2 + (X_j^{\text{add}})^2). \end{aligned} \quad (\text{C19})$$

It is rewritten in the form

$$H_{\text{add}}(s_j) = B_j^{\text{add}} s_j + E_j^{\text{add}}, \quad (\text{C20})$$

with

$$B_j^{\text{add}} = \kappa X_0 X_j^{\text{add}}, \quad E_j^{\text{add}} = \frac{\kappa}{2} (X_0^2 + (X_j^{\text{add}})^2). \quad (\text{C21})$$

Hence, it is possible to control the $B_j s_j$ term by using the $B_j^{\text{add}} s_j$ term because X_{add} can be positive or negative.

In order to cancel the $B_j s_j$ term, it is enough to set

$$\kappa X_j^{\text{add}} = \frac{\varepsilon_0 S V_j^2}{(X_{\text{cap}}^2 - 4X_0^2)}. \quad (\text{C22})$$

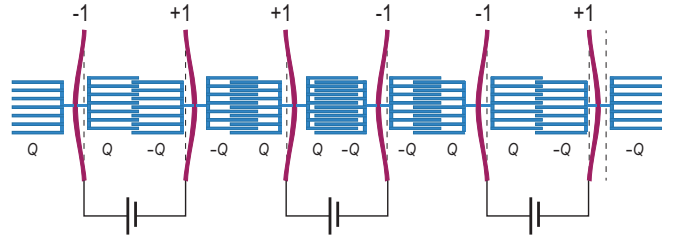


FIG. 14. Illustration of a comb-teeth MEMS, where the direction of buckling is controlled by the charge stored in a comb-teeth MEMS. The charge is supplied externally to the capacitor. Here a homogeneous charge is assumed.

where we have used Eq.(C14). We now obtain the pure Ising Hamiltonian,

$$H'_{\text{Ising}} = \sum_{j=1}^{N-1} J_j s_j s_{j+1} + E_0, \quad (\text{C23})$$

where the $B_j s_j$ terms are absent. We have shown that the presence of randomness is remedied by tuning additional springs.

Appendix D: Characteristic frequency

We estimate the highest frequency of the dynamics. The highest frequency is given by the oscillation at the bottom of the potential (1) at $u_j = \pm X_0$. The potential is expanded around $u_j = X_0$ as

$$U_{\text{mech}}^{(j)} \equiv \frac{\alpha}{2} (u_j^2 - X_0^2)^2 \simeq 2\alpha X_0^2 (u_j - X_0)^2. \quad (\text{D1})$$

The equation of motion is given by

$$m\ddot{u}_j + \gamma\dot{u}_j = -4\alpha X_0^2 (u_j - X_0). \quad (\text{D2})$$

The characteristic frequency is obtained as

$$\omega = \sqrt{\frac{4\alpha X_0^2}{m}}. \quad (\text{D3})$$

Appendix E: Square Network of MEMS

A square network is often used in the annealing machine. We show a method to construct two-dimensional networks of MEMS because there is no frustration in one dimensional MEMS array. We show a mechanism to transfer the motion along the x axis to the y axis in Fig.15(a). The two plates are connected by a green spring, where the end points are the edges of plates. The green spring has a natural length L_0 and rotates freely at the end points. We assume the position of the upper plate is $y = Y$ and the length of the plate is $2a$. When the position of the lower plate is left and the position of the

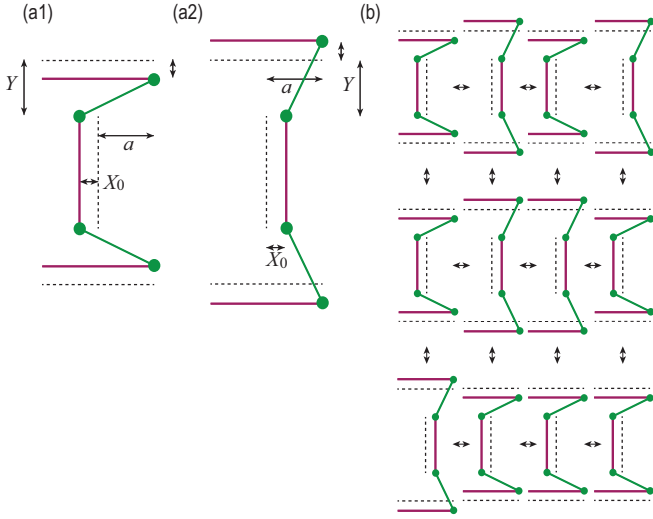


FIG. 15. (a1) and (a2) Illustration of a mechanism connecting the horizontal (x) and vertical (y) motions of MEMS. There are only two configurations, that is (a1) left-down position and (a2) right-up position. (b) A two-dimensional network of MEMS.

upper plate is down as in Fig.15(a1), the length of the green bar is given by

$$L_+ = \sqrt{(X_0 + a)^2 + (Y - X_0)^2}. \quad (\text{E1})$$

In the similar way, when the position of the lower plate is right and the the position of the upper plate is up as in Fig.15(a2), the length of the green bar is given by

$$L_- = \sqrt{(-X_0 + a)^2 + (Y + X_0)^2}. \quad (\text{E2})$$

By equating $L_+ = L_-$, we find that it enough to set $a = Y$. By using this condition, the motion of the lower plate along the x axis is transformed into the y motion of the upper plate.

Next, we consider a network shown in Fig.15(b). There are electrostatic interaction both along the x and y axes. It forms a square network of MEMS.

Appendix F: Comb-teeth MEMS

We have so far considered an Ising machine made of the parallel-plate MEMS. In the current MEMS technology, however, comb-teeth electrostatic actuators (comb-teeth MEMS) are commonly used instead of parallel plate MEMS. It is due to the tradeoff of force, maximum stroke vs stability. Parallel plate actuator can be stably controllable only for $1/3$ of its initial gap X_{cap} . As soon as the displacement u exceeds $X_{\text{cap}}/3$, the plate is continuously pulled until the two plates touch and make short-circuit. This phenomenon is called the pull-in instability. It is because the electrostatic force is inversely proportional to the square of gap: $F(X_{\text{cap}} - u)^{-2}$, whereas the spring counterforces to hold the plate against pull-in is only proportional to its displacement: $F = \kappa u$. On the other hand,

the comb-teeth MEMS machine does not suffer from the pull-in instability because the electrostatic force is constant regardless of the displacement.

It is unnecessary to use metal for buckled plates. We can use plastic or gum for the buckled plates, which extends the possibility of the parameter tuning of the plates. These are merits to overcome the complexity to manufacture the comb-teeth MEMS.

The structure is shown in Fig.14, where many parallel plates form a comb-teeth like structure. The capacitance of the comb-teeth MEMS is proportional to the overlapped area,

$$C_{\text{comb}}(u_j, u_{j+1}) = \frac{\varepsilon_0 d_Y (X_{\text{cap}} + u_j - u_{j+1})}{d_Z}, \quad (\text{F1})$$

where d_Z is the distance between the adjacent plates within the comb-teeth MEMS, and d_Y is the length of the plate of the comb-teeth MEMS along the y direction.

Here we control charge Q_j stored in j -th comb-teeth MEMS. The static energy is given by

$$U_{\text{comb}} = \sum_j \frac{Q_j^2}{2C_{\text{comb}}(u_j, u_{j+1})} \quad (\text{F2})$$

in the presence of a charge Q_j between the j -th and $(j+1)$ -th plates. We consider the configuration shown in Fig.14, where the charge difference is Q_j between the adjacent plates. It is possible to construct an Ising machine based on the comb-teeth MEMS with charge control.

We note that the dynamics is identical between the parallel plates controlling voltage and the comb-teeth MEMS controlling charge by suitably changing variables. Namely, there is a kind of duality between the two systems, as we now show.

Appendix G: Duality

We have shown that the Ising machine may be constructed with the use of the parallel MEMS by controlling voltage. We have also shown that the Ising machine may be constructed with the use of the comb-teeth MEMS by controlling charge. We argue that there is a duality relation between these two systems.

The differences between two types of MEMS are the electrostatic potentials Eq.(C2) under the constant voltage and Eq.(F2) under the constant charge, i.e.,

$$U_{\text{para}} = \sum_j \frac{C_{\text{para}}(u_j, u_{j+1})}{2} V_j^2, \quad (\text{G1})$$

$$U_{\text{comb}} = \sum_j \frac{Q_j^2}{2C_{\text{comb}}(u_j, u_{j+1})}. \quad (\text{G2})$$

They are explicitly given by

$$U_{\text{para}} = \frac{\varepsilon_0 S}{X_{\text{cap}} + u_j - u_{j+1}} \frac{V_j^2}{2}, \quad (\text{G3})$$

$$U_{\text{cap}} = \frac{d_Z}{\varepsilon_0 d_Y (X_{\text{cap}} + u_j - u_{j+1})} \frac{Q_j^2}{2}. \quad (\text{G4})$$

These two potentials are transformed into one another by

$$V_j \Leftrightarrow Q_j, \quad \varepsilon_0 S \Leftrightarrow \frac{d_Z}{\varepsilon_0 d_Y}. \quad (\text{G5})$$

This is the duality relation between the parallel-plate MEMS and the comb-teeth MEMS. All numerical results of the parallel-plate MEMS are applicable to the comb-teeth MEMS by changing parameters according to Eq.(G5).

Appendix H: Explicit equations of motions for fully-connected systems

The equations of motion corresponding to Fig.8(a4) are given by

$$m\ddot{u}_1 + \gamma\dot{u}_1 + 2\alpha u_1 (u_1^2 - X_0) = \frac{\varepsilon_0 S V_{12}^2}{(X_{\text{cap}} + u_1 - u_2)^2} + \frac{\varepsilon_0 S V_{13}^2}{(X_{\text{cap}} + u_1 - u_3)^2} + \frac{\varepsilon_0 S V_{14}^2}{(X_{\text{cap}} + u_1 - u_4)^2} + \frac{\varepsilon_0 S V_{15}^2}{(X_{\text{cap}} + u_1 - u_5)^2}, \quad (\text{H1})$$

$$m\ddot{u}_2 + \gamma\dot{u}_2 + 2\alpha u_2 (u_2^2 - X_0) = -\frac{\varepsilon_0 S V_{12}^2}{(X_{\text{cap}} + u_1 - u_2)^2} + \frac{\varepsilon_0 S V_{23}^2}{(X_{\text{cap}} + u_2 - u_3)^2} + \frac{\varepsilon_0 S V_{24}^2}{(X_{\text{cap}} + u_2 - u_4)^2} + \frac{\varepsilon_0 S V_{25}^2}{(X_{\text{cap}} + u_2 - u_5)^2}, \quad (\text{H2})$$

$$m\ddot{u}_3 + \gamma\dot{u}_3 + 2\alpha u_3 (u_3^2 - X_0) = -\frac{\varepsilon_0 S V_{13}^2}{(X_{\text{cap}} + u_1 - u_3)^2} - \frac{\varepsilon_0 S V_{23}^2}{(X_{\text{cap}} + u_2 - u_3)^2} + \frac{\varepsilon_0 S V_{34}^2}{(X_{\text{cap}} + u_3 - u_4)^2} + \frac{\varepsilon_0 S V_{35}^2}{(X_{\text{cap}} + u_3 - u_5)^2}, \quad (\text{H3})$$

$$m\ddot{u}_4 + \gamma\dot{u}_4 + 2\alpha u_4 (u_4^2 - X_0) = -\frac{\varepsilon_0 S V_{14}^2}{(X_{\text{cap}} + u_1 - u_4)^2} - \frac{\varepsilon_0 S V_{24}^2}{(X_{\text{cap}} + u_2 - u_4)^2} - \frac{\varepsilon_0 S V_{34}^2}{(X_{\text{cap}} + u_3 - u_4)^2} + \frac{\varepsilon_0 S V_{45}^2}{(X_{\text{cap}} + u_4 - u_5)^2}, \quad (\text{H4})$$

$$m\ddot{u}_5 + \gamma\dot{u}_5 + 2\alpha u_5 (u_5^2 - X_0) = -\frac{\varepsilon_0 S V_{15}^2}{(X_{\text{cap}} + u_1 - u_5)^2} - \frac{\varepsilon_0 S V_{25}^2}{(X_{\text{cap}} + u_2 - u_5)^2} - \frac{\varepsilon_0 S V_{35}^2}{(X_{\text{cap}} + u_3 - u_5)^2} - \frac{\varepsilon_0 S V_{45}^2}{(X_{\text{cap}} + u_4 - u_5)^2}. \quad (\text{H5})$$

The equations of motion corresponding to Fig.8(a5) are given by

$$m\ddot{u}_1 + \gamma\dot{u}_1 + 2\alpha u_1 (u_1^2 - X_0) = -\frac{\varepsilon_0 S V_j^2}{(X_{\text{cap}} + u_1 - u_2)^2} + \frac{\varepsilon_0 S V_j^2}{(X_{\text{cap}} + u_1 - u_3)^2} + \frac{\varepsilon_0 S V_j^2}{(X_{\text{cap}} + u_1 - u_4)^2} + \frac{\varepsilon_0 S V_j^2}{(X_{\text{cap}} + u_1 - u_5)^2}, \quad (\text{H6})$$

$$m\ddot{u}_2 + \gamma\dot{u}_2 + 2\alpha u_2 (u_2^2 - X_0) = -\frac{\varepsilon_0 S V_j^2}{(X_{\text{cap}} + u_2 - u_1)^2} + \frac{\varepsilon_0 S V_j^2}{(X_{\text{cap}} + u_2 - u_3)^2} + \frac{\varepsilon_0 S V_j^2}{(X_{\text{cap}} + u_2 - u_4)^2} + \frac{\varepsilon_0 S V_j^2}{(X_{\text{cap}} + u_2 - u_5)^2}, \quad (\text{H7})$$

$$m\ddot{u}_3 + \gamma\dot{u}_3 + 2\alpha u_3 (u_3^2 - X_0) = -\frac{\varepsilon_0 S V_j^2}{(X_{\text{cap}} + u_1 - u_3)^2} - \frac{\varepsilon_0 S V_j^2}{(X_{\text{cap}} + u_2 - u_3)^2} + \frac{\varepsilon_0 S V_j^2}{(X_{\text{cap}} + u_3 - u_4)^2} + \frac{\varepsilon_0 S V_j^2}{(X_{\text{cap}} + u_3 - u_5)^2}, \quad (\text{H8})$$

$$m\ddot{u}_4 + \gamma\dot{u}_4 + 2\alpha u_4 (u_4^2 - X_0) = -\frac{\varepsilon_0 S V_j^2}{(X_{\text{cap}} + u_1 - u_4)^2} - \frac{\varepsilon_0 S V_j^2}{(X_{\text{cap}} + u_2 - u_4)^2} - \frac{\varepsilon_0 S V_j^2}{(X_{\text{cap}} + u_3 - u_4)^2} + \frac{\varepsilon_0 S V_j^2}{(X_{\text{cap}} + u_4 - u_5)^2}, \quad (\text{H9})$$

$$m\ddot{u}_5 + \gamma\dot{u}_5 + 2\alpha u_5 (u_5^2 - X_0) = -\frac{\varepsilon_0 S V_j^2}{(X_{\text{cap}} + u_1 - u_5)^2} - \frac{\varepsilon_0 S V_j^2}{(X_{\text{cap}} + u_2 - u_5)^2} - \frac{\varepsilon_0 S V_j^2}{(X_{\text{cap}} + u_3 - u_5)^2} - \frac{\varepsilon_0 S V_j^2}{(X_{\text{cap}} + u_4 - u_5)^2}. \quad (\text{H10})$$

The equations of motion corresponding to Fig.8(a6) are given by

$$m\ddot{u}_1 + \gamma\dot{u}_1 + 2\alpha u_1 (u_1^2 - X_0) = -\frac{\varepsilon_0 S V_j^2}{(X_{\text{cap}} + u_1 - u_2)^2} + \frac{\varepsilon_0 S V_j^2}{(X_{\text{cap}} + u_1 - u_3)^2} + \frac{\varepsilon_0 S V_j^2}{(X_{\text{cap}} + u_1 - u_4)^2} + \frac{\varepsilon_0 S V_j^2}{(X_{\text{cap}} + u_1 - u_5)^2}, \quad (\text{H11})$$

$$m\ddot{u}_2 + \gamma\dot{u}_2 + 2\alpha u_2 (u_2^2 - X_0) = -\frac{\varepsilon_0 S V_j^2}{(X_{\text{cap}} + u_2 - u_1)^2} + \frac{\varepsilon_0 S V_j^2}{(X_{\text{cap}} + u_2 - u_3)^2} + \frac{\varepsilon_0 S V_j^2}{(X_{\text{cap}} + u_2 - u_4)^2} + \frac{\varepsilon_0 S V_j^2}{(X_{\text{cap}} + u_2 - u_5)^2}, \quad (\text{H12})$$

$$m\ddot{u}_3 + \gamma\dot{u}_3 + 2\alpha u_3 (u_3^2 - X_0) = -\frac{\varepsilon_0 S V_j^2}{(X_{\text{cap}} + u_1 - u_3)^2} - \frac{\varepsilon_0 S V_j^2}{(X_{\text{cap}} + u_2 - u_3)^2} + \frac{\varepsilon_0 S V_j^2}{(X_{\text{cap}} + u_3 - u_4)^2} + \frac{\varepsilon_0 S V_j^2}{(X_{\text{cap}} + u_3 - u_5)^2}, \quad (\text{H13})$$

$$m\ddot{u}_4 + \gamma\dot{u}_4 + 2\alpha u_4 (u_4^2 - X_0) = -\frac{\varepsilon_0 S V_j^2}{(X_{\text{cap}} + u_1 - u_4)^2} - \frac{\varepsilon_0 S V_j^2}{(X_{\text{cap}} + u_2 - u_4)^2} - \frac{\varepsilon_0 S V_j^2}{(X_{\text{cap}} + u_3 - u_4)^2} + \frac{\varepsilon_0 S V_j^2}{(X_{\text{cap}} + u_4 - u_5)^2}, \quad (\text{H14})$$

$$m\ddot{u}_5 + \gamma\dot{u}_5 + 2\alpha u_5 (u_5^2 - X_0) = -\frac{\varepsilon_0 S V_j^2}{(X_{\text{cap}} + u_1 - u_5)^2} - \frac{\varepsilon_0 S V_j^2}{(X_{\text{cap}} + u_2 - u_5)^2} - \frac{\varepsilon_0 S V_j^2}{(X_{\text{cap}} + u_3 - u_5)^2} - \frac{\varepsilon_0 S V_j^2}{(X_{\text{cap}} + u_5 - u_4)^2}. \quad (\text{H15})$$

-
- [1] A. Lucas, *Frontiers in Physics* 2, 5 (2014)
- [2] S. Kirkpatrick, Jr. C. D. Gelatt, M. P. Vecchi, *Science* **220**, 671 (1983).
- [3] V. Cerny, *J. Opt. Theory and Applications* **45** 41 (1985)
- [4] T. Kadowaki and H. Nishimori, *Phys. Rev. E* **58**, 5355 (1998)
- [5] E. Farhi, J. Goldstone, S. Gutmann, J. Lapan, A. Ludgren and D. Preda, *Science* **292**, 472 (2001)
- [6] M. W. Johnson, M. H. S. Amin, G. Rose, *Nature* **473**, 194 (2011)
- [7] R. Afoakwa, Y. Zhang, U. Kumar, R. Vengalam, Z. Ignjatovic and M. Huang, "BRIM: Bistable Resistively-Coupled Ising Machine" 2021 IEEE International Symposium on High-Performance Computer Architecture (HPCA) (2021)
- [8] S. Utsunomiya, K. Takata and Y. Yamamoto, *Opt. Express* **19**, 18091 (2011).
- [9] Z. Wang, A. Marandi, K. Wen, R. L. Byer and Y. Yamamoto, *Phys. Rev. A* **88**, 063853 (2013).
- [10] A. Marandi, Z. Wang, K. Takata, R. L. Byer and Y. Yamamoto, *Nature Photonics* **8**, 937 (2014).
- [11] T. Inagaki, Y. Haribara, K. Igarashi, T. Sonobe, S. Tamate, T. Honjo, A. Marandi, P. L. McMahon, T. Umeki, K. Enbutsu, O. Tadanaga, H. Takenouchi, K. Aihara, K.-i. Kawarabayashi, K. Inoue, S. Utsunomiya, H. Takesue, *Science* **354** 603 (2016)
- [12] F. Bohm, G. Verschaffelt and G. V. der Sande, *Nat. Com* **10**, 3538 (2019)
- [13] T. Wang and J. Roychowdhury, "OIM: Oscillator-Based Ising Machines for Solving Combinatorial Optimisation Problems," (2019).
- [14] M. Yamaoka, C. Yoshimura, M. Hayashi, T. Okuyama, H. Aoki and H. Mizuno, "24.3 20k-spin ising chip for combinational optimization problem with cmos annealing," IEEE International Solid-State Circuits Conference - (ISSCC) Digest of Technical Papers (2015)
- [15] T. Takemoto, M. Hayashi, C. Yoshimura, and M. Yamaoka, "2.6 a 2 by 30k-spin multichip scalable annealing processor based on a processing-in-memory approach for solving large-scale combinatorial optimization problems," in IEEE International Solid-State Circuits Conference, (2019)
- [16] H. Goto, *Sci. Rep.* **6**, 21686 (2016)
- [17] H. Goto, *J. Phys. Soc. Jpn.* **88**, 061015 (2019)
- [18] W. A. Borders, A. Z. Pervaiz, S. Fukami, K. Y. Camsari, H. Ohno, and S. Datta, *Nature* **573**, 390 (2019)
- [19] K. Y. Camsari, S. Chowdhury and S. Datta, *Phys. Rev. Applied* **12**, 034061 (2019)
- [20] K. Y. Camsari, B. M. Sutton and S. Datta, *Applied Physics Reviews* **6**, 011305 (2019)
- [21] A. Z. Pervaiz, B. M. Sutton, L. A. Ghantasala and K. Y. Camsari, *IEEE Transactions on Neural Networks and Learning Systems* **30** 1920 (2019)
- [22] K. Y. Camsari, M. M. Torunbalci, W. A. Borders, H. Ohno and S. Fukami *Phys. Rev. Applied* **15**, 044049 (2021)
- [23] R. P. Feynman, *Int. J. Theoretical Physics* **21**, 467 (1982)
- [24] Y. Mita, A. Hirakawa, B. Stefanelli, I. Mori, Y. Okamoto, S. Morishita, M. Kubota, E. Lebrasseur, A. Kaiser, *Japanese Journal of Applied Physics* **57**, 04FA05 (2018)
- [25] R. Reddy, K. Komeda, Y. Okamoto, E. Lebrasseur, A. Higo, Y. Mita, *Sensors and Actuators A: Physical*, **295**, 1 (2019)
- [26] H. Toshiyoshi, *Electrostatic Actuation*. In: Yogesh B Gianchandani, Osamu Tabata, Hans Zappe, (Editors in Chief) *Comprehensive Microsystems*, **2**, 1 Amsterdam: Elsevier. (2008)
- [27] S. F. Edwards and P. W. Anderson *J. Phys. F: Met. Phys.* **5**, 965 (1975)
- [28] M. Vangbo, *Sensors and Actuators A: Physical* **69**, 212 (1998)
- [29] V. Intaraprasongk and S. Fan, *Appl. Phys. Lett.* **98**, 241104 (2011)
- [30] J. Martinez-Rincon and Y. V. Pershin, *IEEE Transactions on Electron Devices* **58**, 1809 (2011)
- [31] V. Choi, *Quantum Information Processing* volume **10**, 343 (2011).
- [32] D. Oku, K. Terada, M. Hayashi, M. Yamaoka, S. Tanaka and N. Togawa, *IEICE TRANS. INF. and SYST.*, E102 D , 1696 (2019).

- [33] I. Mahboob, H. Okamoto and H. Yamaguchi, *Science Advances* 2, e1600236 (2016).
- [34] Y. Mita, E. Lebrasseur, M. Ezawa, K. Tsuji, M. Kawamura and A. Higo, "*TopoMEMS circuit: step-variable-resettable MEMS capacitor for topological electrical circuit*", The 21st International Conference on Solid-State Sensors, Actuators and Microsystems (Transducers), 20-25 June, online (2021) DOI:10.1109/Transducers50396.2021.9495418
- [35] Y. Mita, M. Ezawa, K. Tsuji, E. Lebrasseur, T. Sawamura, S. Tsuboi, A. Mizushima, Y. Ochiai and A. Higo, "*Test Structure of Bi-stable Spring towards TopoMEMS Ising Machine*" 21-24 March, online (2022) IEEE ICMTS (2022)